

# SAR Despeckling using a Denoising Diffusion Probabilistic Model

Malsha V. Perera, *Student Member, IEEE*, Nithin Gopalakrishnan Nair, *Student Member, IEEE*, Wele Gedara Chaminda Bandara, *Student Member, IEEE* and Vishal M. Patel, *Senior Member, IEEE*

**Abstract**—Speckle is a multiplicative noise which affects all coherent imaging modalities including Synthetic Aperture Radar (SAR) images. The presence of speckle degrades the image quality and adversely affects the performance of SAR image understanding applications such as automatic target recognition and change detection. Thus, SAR despeckling is an important problem in remote sensing. In this paper, we introduce SAR-DDPM, a denoising diffusion probabilistic model for SAR despeckling. The proposed method comprises of a Markov chain that transforms clean images to white Gaussian noise by repeatedly adding random noise. The despeckled image is recovered by a reverse process which iteratively predicts the added noise using a noise predictor which is conditioned on the speckled image. In addition, we propose a new inference strategy based on cycle spinning to improve the despeckling performance. Our experiments on both synthetic and real SAR images demonstrate that the proposed method achieves significant improvements in both quantitative and qualitative results over the state-of-the-art despeckling methods. The code is available at: [https://github.com/malshaV/SAR\\_DDPM](https://github.com/malshaV/SAR_DDPM)

**Index Terms**—Synthetic Aperture Radar, diffusion models, speckle, denoising

## I. INTRODUCTION

**S**YNTHETIC Aperture Radar (SAR) is a coherent imaging modality which is strongly invariant to different environmental conditions. Therefore, SAR is widely used in applications such as landscape classification, disaster monitoring, and surface change detection. Nonetheless, SAR images are often affected by speckle which is a signal-dependent, spatially correlated noise. While degrading the SAR images, the presence of speckle creates an adverse effect on downstream tasks. Hence, several methods for speckle removal have been proposed in the literature for enhancing the SAR images over the past decades.

For a given SAR intensity  $Y$ , the mathematical model of multiplicative speckle noise  $N$  can be expressed as follows:

$$Y = XN, \quad (1)$$

where  $X$  is the speckle-free or the clean image. Generally, it is assumed that  $N$  follows a Gamma distribution with unit mean and variance of  $1/L$ , with the following probability density function:

$$p(N) = \frac{1}{\Gamma(N)} L^L N^{L-1} e^{-LN}, \quad (2)$$

This work was supported by the NSF CAREER Award under Grant 2045489.

M. V. Perera, N. G. Nair, W. G. C. Bandara, and V. M. Patel are with the Department of Electrical and Computer Engineering, Johns Hopkins University, Baltimore, MD, 21218. (e-mail: {jperera4, ngopala2, wbandar1, and vpatel36}@jhu.edu).

where  $\Gamma(\cdot)$  is the Gamma function and  $L$  is the number of looks in multilook processing.

The first attempts at despeckling employed spatial domain filtering-based approaches such as Lee filter [1], Kuan filter [2] and Gamma maximum a *posteriori* (MAP) filter [3]. These approaches generally use the spatial correlation of image to filter noise by employing a sliding window to compute the pixel value at the center of the window. However, these methods result in intense smoothing and most edges and texture details in the SAR images are lost. In 2009, Deledalle *et al.* proposed a probabilistic patch-based (PPB) [4] filtering method which combines non-local means filtering and 3-D block matching approach (BM3D) [5]. Parrilli *et al.* [6] introduced SAR-BM3D for SAR despeckling by extending BM3D. Sparse dictionary-based despeckling methods have also been proposed in the literature [7]. A detailed review of SAR despeckling approaches can be found in [8] and [9].

More recently, deep learning algorithms have gained popularity and achieved state-of-the-art performance in wide range of computer vision and image processing tasks. Following this trend, several studies have attempted to apply deep networks for SAR despeckling. SAR-CNN [10] is one of the earliest Convolutional Neural Network (CNN) based despeckling methods. This method transforms the multiplicative speckle noise to additive noise applying a homomorphic transformation to the SAR images. In order to train the network, SAR-CNN uses multi-temporal fusion to generate clean reference images. Wang *et al.* [11] proposed ID-CNN which is trained on synthetically speckled optical images. ID-CNN uses a residual network architecture, which obtains despeckled image by dividing the input speckled image by the estimated speckle. ID-GAN proposed in [12], uses a Generative Adversarial Network (GAN) [13] for despeckling which is trained using a combination of Euclidean loss, Perceptual loss and Adversarial loss. In addition to training deep learning models using spatial loss functions, the Multi-Objective network (MONet) [14] incorporates a loss function that computes Kullback–Leibler divergence between the the predicted and simulated speckle probability distribution. Studies such as multiscale residual dense dual attention network (MRDDANet) [15] and SAR-CAM [16] incorporate various attention modules in the network architecture for despeckling. In [17], an overcomplete CNN architecture (SAR-ON) which focuses on learning low-level features by restricting the receptive field is used for SAR despeckling. Apart from CNN architectures, [18] introduces a Transformer-based architecture (Trans-SAR) for despeckling of SAR images.

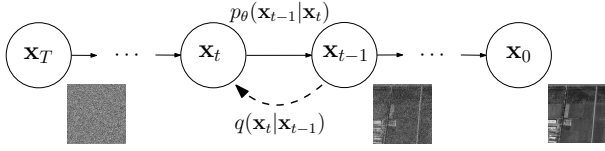


Fig. 1. Overview of the forward and reverse diffusion process

Recently, Denoising Diffusion Probabilistic Models (DDPM) [19] have emerged as an alternative approach for generative modelling. Dhariwal and Nichol [20] successfully presented that DDPM can outperform the current state-of-the-art GAN-based generative models [13] in image synthesis. DDPM is parameterized by a Markov chain that gradually adds noise to the data until the signal is destroyed. During inference, a sample belonging to the training distribution can be generated by starting with a randomly sampled Gaussian noise and iteratively applying a reverse diffusion step. DDPM is trained by optimizing the variational lower bound of the negative log-likelihood of the data, and it avoids the mode collapse often encountered by GANs. With the success in image synthesis tasks, DDPMs have been adopted into a variety of vision tasks such as super-resolution [21], in-painting [22] and image restoration [23]. To the best of our knowledge, SAR despeckling based on Denoising Diffusion Probabilistic Models has not been studied in the literature.

Inspired by these studies, we propose SAR-DDPM, a Denoising Diffusion Probabilistic Model-based approach for SAR despeckling. In our approach, we iteratively recover the clean image by employing a noise predictor conditioned on the speckled image. We train the proposed DDPM model with synthetically speckled optical images and test our approach on both synthetic and real SAR images. During inference, we incorporate a novel strategy based on cycle spinning [24] to improve the despeckling performance. Finally, we demonstrate the effectiveness of our method on synthetic and real SAR images by comparing with several recent despeckling approaches.

## II. PROPOSED METHOD

### A. Denoising Diffusion Probabilistic Models

Denoising Diffusion Probabilistic Models define a Markov chain that transforms an image  $\mathbf{x}_0$  to white Gaussian Noise  $\mathbf{x}_T \sim \mathcal{N}(0, 1)$  by adding random noise in  $T$  diffusion time steps. During inference, a random noise vector  $\mathbf{x}_T$  is sampled and gradually denoised until it reaches the desired image  $\mathbf{x}_0$ . As illustrated in Fig. 1, DDPM comprises of two processes: a forward diffusion process and a reverse diffusion process.

In the forward diffusion process,  $\mathbf{x}_0 \sim q(\mathbf{x})$  sampled from the real data distribution is converted to  $\mathbf{x}_T$  by gradually adding Gaussian noise  $\epsilon$  according to a variance schedule  $\beta_1, \dots, \beta_T$

$$q(\mathbf{x}_t | \mathbf{x}_{t-1}) = \mathcal{N}(\mathbf{x}_t; \sqrt{1 - \beta_t} \mathbf{x}_{t-1}, \beta_t \mathbf{I}), \quad (3)$$

$$q(\mathbf{x}_{1:T} | \mathbf{x}_0) = \prod_{t=1}^T q(\mathbf{x}_t | \mathbf{x}_{t-1}). \quad (4)$$

In the forward process,  $\mathbf{x}_t$  can be sampled at any arbitrary time step  $t$  by setting  $\alpha_t = 1 - \beta_t$  and  $\bar{\alpha}_t = \prod_{i=1}^t \alpha_i$

$$q(\mathbf{x}_t | \mathbf{x}_0) = \mathcal{N}(\mathbf{x}_t; \bar{\alpha}_t \mathbf{x}_0, (1 - \bar{\alpha}_t) \mathbf{I}). \quad (5)$$

This can be further reparameterized as follows

$$\mathbf{x}_t = \sqrt{\bar{\alpha}_t} \mathbf{x}_0 + \sqrt{1 - \bar{\alpha}_t} \epsilon, \quad \epsilon \sim \mathcal{N}(0, 1). \quad (6)$$

The reverse diffusion process is modeled by a neural network trained to predict the parameters  $\mu_\theta(\mathbf{x}_t, t)$  and  $\Sigma_\theta(\mathbf{x}_t, t)$  of a Gaussian distribution

$$p_\theta(\mathbf{x}_{t-1} | \mathbf{x}_t) = \mathcal{N}(\mathbf{x}_{t-1}; \mu_\theta(\mathbf{x}_t, t), \Sigma_\theta(\mathbf{x}_t, t)). \quad (7)$$

As reported by Ho *et al.* [19], learning objective for the above model is derived by considering the variational lower bound,

$$\begin{aligned} \mathbb{E}[p_\theta(\mathbf{x}_0)] \leq L = & \mathbb{E}_q \left[ \underbrace{D_{KL}(q(\mathbf{x}_T | \mathbf{x}_0) || p(\mathbf{x}_T))}_{L_T} \right. \\ & \left. + \sum_{t>1} \underbrace{D_{KL}(q(\mathbf{x}_{t-1} | \mathbf{x}_t, \mathbf{x}_0) || p(\mathbf{x}_{t-1} | \mathbf{x}_t))}_{L_{t-1}} \underbrace{- \log p_\theta(\mathbf{x}_0 | \mathbf{x}_1)}_{L_0} \right]. \end{aligned} \quad (8)$$

Note that the term  $L_{t-1}$  is used to train the neural network and this can be computed in closed form as  $L_{t-1}$  compares two Gaussian distributions. As  $\mathbf{x}_t$  is available as an input during training, the predicted mean  $\mu_\theta(\mathbf{x}_t, t)$  can be reparameterized as follows,

$$\mu_\theta(\mathbf{x}_t, t) = \frac{1}{\sqrt{\bar{\alpha}_t}} \left( \mathbf{x}_t - \frac{\beta_t}{\sqrt{1 - \bar{\alpha}_t}} \epsilon_\theta(\mathbf{x}_t, t) \right). \quad (9)$$

For simplicity, Ho *et al.* [19] derive the following training objective from  $L_{t-1}$  in Eq. (8).

$$L_{simple} = \mathbb{E}_{t, \mathbf{x}_0, \epsilon} [\|\epsilon - \epsilon_\theta(\mathbf{x}_t, t)\|^2]. \quad (10)$$

### B. SAR-DDPM

The proposed method is based on a  $T$  step DDPM model with a forward and a reverse diffusion processes as shown in Fig. 1. During the forward diffusion process, we use the clean image  $\mathbf{x}_C$  as the input image  $\mathbf{x}_0$  which is converted into  $\mathbf{x}_T$  by gradually adding a Gaussian noise. The reverse process uses the conditional noise predictor  $\epsilon_\theta$  to recover the clean image  $\mathbf{x}_C$  from  $\mathbf{x}_T$  by denoising iteratively in  $T$  steps.

In the proposed method, the conditional noise predictor  $\epsilon_\theta$  is trained to predict the noise added in each diffusion step conditioned on the speckled image  $\mathbf{x}_S$ . The network architecture of the proposed conditional noise predictor is illustrated in Fig. 2. The proposed network follows a U-Net [25] like architecture which comprises of convolutional residual blocks, attention blocks, downsampling convolutions, upsampling convolutions, and skip connections connecting the contracting and expansive pathways. First, the speckled image  $\mathbf{x}_S$  and  $\mathbf{x}_t$  are concatenated and passed through a convolutional layer, while the timestep  $t$  is transformed to the timestep embedding  $t_e$  using the transformer sinusoidal positional encoding [26]. The time step embedding  $t_e$  is given as an input to each residual block as depicted in Fig. 2. Similar to [20], we use self-attention blocks at multiple resolutions,

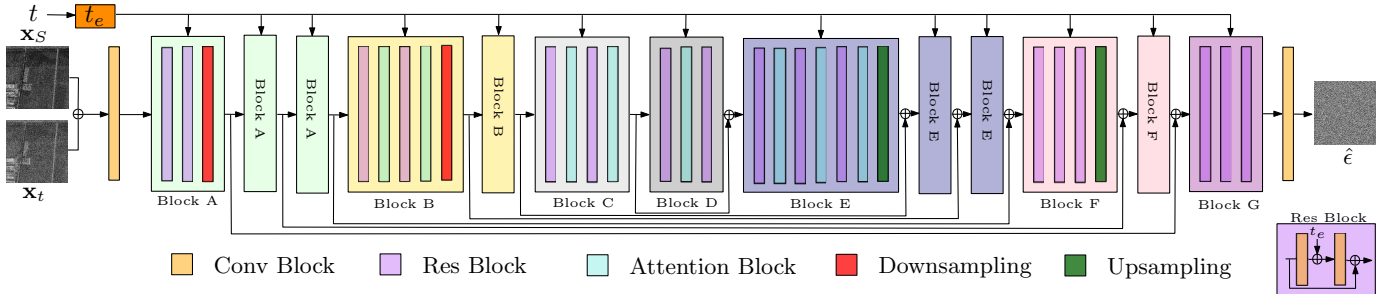


Fig. 2. Overview of the conditional noise predictor network architecture in SAR-DDPM. Here, 2D-Convolution block, and residual block are denoted as “Conv Block”, and “Res Block”, respectively.

and BigGAN [27] residual blocks for upsampling and downsampling. Finally, the output from the last residual block of the expansive pathway is passed through a convolutional block to predict the noise  $\hat{\epsilon}$  at the time step  $t-1$ . The predicted noise is then used to obtain  $\mathbf{x}_{t-1}$  using Eq. (7) and (9).

Algorithm 1 summarises the training procedure of the proposed method where synthetically speckled images and their corresponding clean images are used to train the SAR-DDPM in  $T$  diffusion steps. During inference, we adopt the idea of cycle spinning [24] to improve the performance of SAR-DDPM. The function  $f_{cs}(\cdot, u, v)$  is used to shift an image cyclically by  $u$  rows and  $v$  columns as depicted in Fig. 3. We despeckle the cyclically shifted images using the DDPM model, apply inverse cyclic shift, and average them to obtain the final despeckled image. The complete inference procedure is given in Algorithm 2.

---

#### Algorithm 1 Training

---

**Input:** Speckled image and clean image pairs  $P = \{(\mathbf{x}_S^k, \mathbf{x}_C^k)\}_{k=1}^K$

- 1: **repeat**
- 2:  $(\mathbf{x}_S, \mathbf{x}_C) \sim P$
- 3:  $t \sim \text{Uniform}(\{1, \dots, T\})$
- 4:  $\epsilon \sim \mathcal{N}(\mathbf{0}, \mathbf{I})$
- 5: Take gradient descent step on  $\nabla_{\theta} \|\epsilon - \epsilon_{\theta}(\mathbf{x}_t, \mathbf{x}_S, t)\|^2$ ,  
 $\mathbf{x}_t = \sqrt{\alpha_t} \mathbf{x}_C + \sqrt{1 - \alpha_t} \epsilon$
- 6: **until** converged

---



---

#### Algorithm 2 Inference

---

**Input:** Speckled image  $\mathbf{x}_S$ ,  $\{u_i\}_{i=1}^M$ ,  $\{v_i\}_{i=1}^M$

- 1: **for**  $i = 1, \dots, M$  **do**
- 2:  $\mathbf{x}_i = f_{cs}(\mathbf{x}_S, u_i, v_i)$
- 3: Sample  $\mathbf{x}_T \sim \mathcal{N}(\mathbf{0}, \mathbf{I})$
- 4: **for**  $t = T, \dots, 1$  **do**
- 5: sample  $\mathbf{z} \sim \mathcal{N}(\mathbf{0}, \mathbf{I})$  if  $t > 1$  else  $\mathbf{z} = \mathbf{0}$
- 6: compute  $\mathbf{x}_{t-1} = \frac{1}{\sqrt{\alpha_t}} \left( \mathbf{x}_t - \frac{1 - \alpha_t}{\sqrt{1 - \alpha_t}} \epsilon_{\theta}(\mathbf{x}_t, \mathbf{x}_i, t) \right) + \sigma_t \mathbf{z}$
- 7: **end for**
- 8:  $\mathbf{x}_{C_i} = f_{cs}^{-1}(\mathbf{x}_0, u_i, v_i)$
- 9:  $\mathbf{x}_{sum} = \mathbf{x}_{sum} + \mathbf{x}_{C_i}$  if  $i > 1$  else  $\mathbf{x}_{sum} = \mathbf{x}_{C_i}$
- 10: **end for**
- 11: **return**  $\mathbf{x}_C = \frac{\mathbf{x}_{sum}}{M}$

---

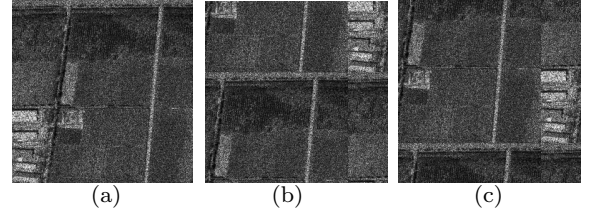


Fig. 3. Cyclically spun images with : (a)  $u = 0, v = 0$  (Original speckled image), (b)  $u = 100, v = 200$ , and (c)  $u = 200, v = 200$

### III. EXPERIMENTS AND RESULTS

In this section, we present the experiments and results of our proposed method on both synthetically speckled images and real SAR images. We compare the performance of SAR-DDPM with the following despeckling algorithms: PPB [4], SAR-BM3D [6], ID-CNN [11], Trans-SAR [18], SAR-ON [17], and SAR-CAM [16]. Following Eq. (1) and (2), we created single-look ( $L = 1$ ) synthetic speckle images using 15k remote sensing images from publicly available DSIFN [28] dataset in order to train SAR-DDPM. The network was trained on an NVIDIA RTX 2080Ti GPU for 30k iterations and the network weights were initialized with pretrained ImageNet weights from [20]. In this work, we set  $T = 1000$  and  $\{u_i\} = \{v_i\} = \{0, 100, 200\}$ .

Table I shows the performance of the proposed algorithm in terms of average Peak Signal-to-Noise Ratio (PSNR) and Structured Similarity Index (SSIM) on 10 synthetically speckled images from the DSIFN dataset. Note that ID-CNN, Trans-SAR, SAR-ON, and SAR-CAM were also trained on the same synthetic data as the proposed method. As can be seen from Table I, SAR-DDPM significantly outperforms both classical and deep learning-based despeckling methods in terms of PSNR and SSIM. Moreover, by the results in Table I and Fig. 4, we can observe that cycle spinning significantly improves the despeckling performance of SAR-DDPM. Also, it can be seen from Fig. 4 that our proposed method provides a better despeckling performance while preserving the fine structural details present in the speckled images compared to the other despeckling methods.

In order to further evaluate the despeckling ability of our proposed method, the above despeckling methods are tested on 2 single-look SAR images of size  $256 \times 256$  acquired using Sentinel-I [29]. The Equivalent Number of Looks (ENL) is an index suitable for evaluating the level of smoothing in

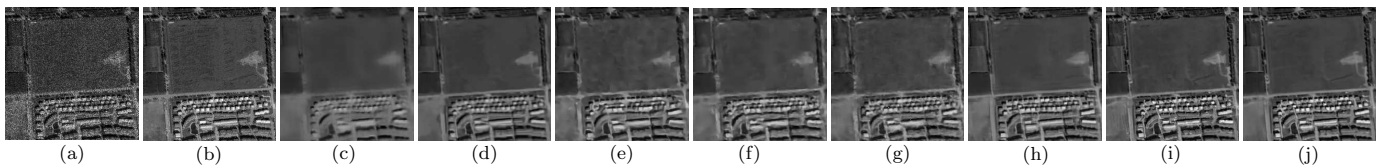


Fig. 4. Results on a synthetically speckled image: (a) Speckled image, (b) Ground Truth, (c) PPB, (d) SAR-BM3D, (e) ID-CNN, (f) Trans-SAR, (g) SAR-ON, (h) SAR-CAM, (i) SAR-DDPM, (j) SAR-DDPM + Cycle Spinning .

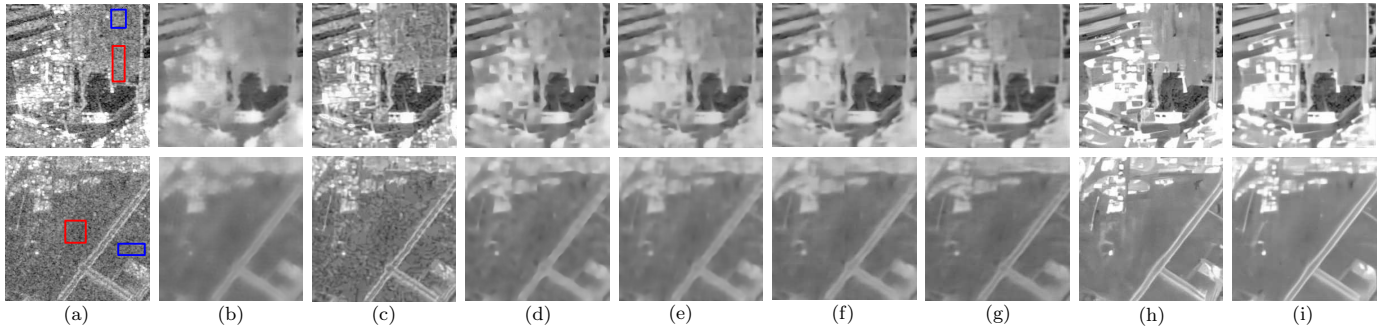


Fig. 5. Results on real SAR images: (a) SAR image, (b) PPB, (c) SAR-BM3D, (d) ID-CNN, (e) Trans-SAR, (f) SAR-ON, (g) SAR-CAM, (h) SAR-DDPM, (i) SAR-DDPM + Cycle Spinning .

TABLE I  
RESULTS ON SYNTHETICALLY SPECKLED IMAGES OF DSIFN.

Method	PSNR	SSIM
PPB [4]	23.96 dB	0.62
SAR-BM3D [6]	25.69 dB	0.75
ID-CNN [11]	27.30 dB	0.72
Trans-SAR [18]	27.08 dB	0.72
SAR-ON [17]	27.16 dB	0.73
SAR-CAM [16]	27.96 dB	0.76
SAR-DDPM	27.99 dB	0.77
SAR-DDPM with cycle spinning	<b>29.42 dB</b>	<b>0.81</b>

homogeneous areas of SAR images when the clean ground truth images are unavailable [30]. ENL is defined as the ratio between the square of the mean and the variance of a homogeneous region. Table II summarizes the quantitative comparison of despeckling results of SAR images in terms of ENL. The regions selected for the ENL value calculation are marked in red and blue boxes in Fig. 5. The proposed method resulted in the highest ENL values in all 4 regions which signifies the best despeckling performance out of the considered despeckling methods. From Fig. 5, we can observe that quantitative results using ENL are consistent with the visual results.

In Fig. 5, the PPB despeckling approach over-smooths the SAR image, destroying edges and structural details. It can also be observed that, SAR-BM3D preserves significantly more details than PPB. However, as indicated by the ENL values, SAR-BM3D exhibits a poor performance when it comes to smoothing. ID-CNN, Trans-SAR, and SAR-ON preserve more textural details than PPB and remove more speckle than SAR-BM3D. Compared to ID-CNN, Trans-SAR and SAR-ON, SAR-CAM retains more textural details while minimizing distortions in homogeneous regions. Even though SAR-CAM showcase a better despeckling ability than the

previous methods, it can be observed that SAR-CAM blurs out some fine edges and structural details. While SAR-DDPM is able to recover these finer details than SAR-CAM, it creates slight distortions in the homogeneous areas resulting in lower ENL values. As evident from Fig. 5 (i), the use of cycle spinning along with SAR-DDPM reduces these distortions and recovers finer structural details than SAR-CAM.

TABLE II  
ESTIMATED ENL VALUES ON REAL SAR IMAGES

Method	Image 1 Red	Image 1 Blue	Image 2 Red	Image 2 Blue
PPB [4]	659.72	622.61	257.50	441.37
SAR-BM3D [6]	100.79	78.87	70.95	80.93
ID-CNN [11]	501.43	394.91	210.65	400.88
Trans-SAR [18]	613.61	485.48	234.69	406.54
SAR-ON [17]	494.63	527.85	255.50	454.36
SAR-CAM [16]	566.20	628.49	271.88	500.11
SAR-DDPM	446.69	301.84	256.39	190.99
SAR-DDPM with cycle spinning	<b>747.92</b>	<b>988.85</b>	<b>372.93</b>	<b>560.61</b>

#### IV. CONCLUSION

We proposed SAR-DDPM, the first diffusion-based model for SAR despeckling. Our work performs despeckling through a novel strategy based upon ensembling multiple cycle spinning based estimates for the despeckled image generated using the diffusion model. Each estimate is obtained by starting from random Gaussian noise and iteratively denoising the latent variables using a noise predictor conditioned on the corresponding transformed speckled images. Our experiments on synthetic and real SAR images show promising quantitative and qualitative improvements compared with several existing despeckling methods. The proposed method proved to be effective in removing speckle while retaining fine structural details in the SAR images.

## REFERENCES

- [1] J.-S. Lee, "Speckle analysis and smoothing of synthetic aperture radar images," *Computer Graphics and Image Processing*, vol. 17, no. 1, pp. 24–32, 1981. [Online]. Available: <https://www.sciencedirect.com/science/article/pii/S0146664X81800056>
- [2] D. T. Kuan, A. A. Sawchuk, T. C. Strand, and P. Chavel, "Adaptive noise smoothing filter for images with signal-dependent noise," *IEEE Transactions on Pattern Analysis and Machine Intelligence*, vol. PAMI-7, no. 2, pp. 165–177, 1985.
- [3] A. Lopes, E. Nezry, R. Touzi, and H. Laur, "Maximum a posteriori speckle filtering and first order texture models in sar images," in *10th Annual International Symposium on Geoscience and Remote Sensing*, 1990, pp. 2409–2412.
- [4] C.-A. Deledalle, L. Denis, and F. Tupin, "Iterative weighted maximum likelihood denoising with probabilistic patch-based weights," *IEEE Transactions on Image Processing*, vol. 18, no. 12, pp. 2661–2672, 2009.
- [5] K. Dabov, A. Foi, V. Katkovnik, and K. Egiazarian, "Image denoising by sparse 3-d transform-domain collaborative filtering," *IEEE Transactions on Image Processing*, vol. 16, no. 8, pp. 2080–2095, 2007.
- [6] S. Parrilli, M. Poderico, C. V. Angelino, and L. Verdoliva, "A nonlocal sar image denoising algorithm based on lmmse wavelet shrinkage," *IEEE Transactions on Geoscience and Remote Sensing*, vol. 50, no. 2, pp. 606–616, 2012.
- [7] V. M. Patel, G. R. Easley, R. Chellappa, and N. M. Nasrabadi, "Separated component-based restoration of speckled sar images," *IEEE Transactions on Geoscience and Remote Sensing*, vol. 52, no. 2, pp. 1019–1029, 2014.
- [8] R. Touzi, "A review of speckle filtering in the context of estimation theory," *IEEE Transactions on Geoscience and Remote Sensing*, vol. 40, no. 11, pp. 2392–2404, 2002.
- [9] C.-A. Deledalle, L. Denis, G. Poggi, F. Tupin, and L. Verdoliva, "Exploiting patch similarity for sar image processing: The nonlocal paradigm," *IEEE Signal Processing Magazine*, vol. 31, no. 4, pp. 69–78, 2014.
- [10] G. Chierchia, D. Cozzolino, G. Poggi, and L. Verdoliva, "Sar image despeckling through convolutional neural networks," in *2017 IEEE International Geoscience and Remote Sensing Symposium (IGARSS)*, 2017, pp. 5438–5441.
- [11] P. Wang, H. Zhang, and V. M. Patel, "Sar image despeckling using a convolutional neural network," *IEEE Signal Processing Letters*, vol. 24, no. 12, pp. 1763–1767, 2017.
- [12] —, "Generative adversarial network-based restoration of speckled sar images," in *2017 IEEE 7th International Workshop on Computational Advances in Multi-Sensor Adaptive Processing (CAMSAP)*, 2017, pp. 1–5.
- [13] I. Goodfellow, J. Pouget-Abadie, M. Mirza, B. Xu, D. Warde-Farley, S. Ozair, A. Courville, and Y. Bengio, "Generative adversarial nets," in *Advances in Neural Information Processing Systems*, Z. Ghahramani, M. Welling, C. Cortes, N. Lawrence, and K. Weinberger, Eds., vol. 27. Curran Associates, Inc., 2014. [Online]. Available: <https://proceedings.neurips.cc/paper/2014/file/5ca3e9b122f61f8f06494c97b1afccf3-Paper.pdf>
- [14] S. Vitale, G. Ferraioli, and V. Pascazio, "Multi-objective cnn-based algorithm for sar despeckling," *IEEE Transactions on Geoscience and Remote Sensing*, vol. 59, no. 11, pp. 9336–9349, 2021.
- [15] S. Liu, Y. Lei, L. Zhang, B. Li, W. Hu, and Y.-D. Zhang, "Mrddanet: A multiscale residual dense dual attention network for sar image denoising," *IEEE Transactions on Geoscience and Remote Sensing*, pp. 1–13, 2021.
- [16] J. Ko and S. Lee, "Sar image despeckling using continuous attention module," *IEEE Journal of Selected Topics in Applied Earth Observations and Remote Sensing*, vol. 15, pp. 3–19, 2022.
- [17] M. V. Perera, W. G. C. Bandara, J. M. J. Valanarasu, and V. M. Patel, "Sar despeckling using overcomplete convolutional networks," 2022. [Online]. Available: <https://arxiv.org/abs/2205.15906>
- [18] —, "Transformer-based sar image despeckling," 2022. [Online]. Available: <https://arxiv.org/abs/2201.09355>
- [19] J. Ho, A. Jain, and P. Abbeel, "Denoising diffusion probabilistic models," in *Advances in Neural Information Processing Systems*, H. Larochelle, M. Ranzato, R. Hadsell, M. Balcan, and H. Lin, Eds., vol. 33. Curran Associates, Inc., 2020, pp. 6840–6851. [Online]. Available: <https://proceedings.neurips.cc/paper/2020/file/4c5bcfec8584af0d967f1ab10179ca4b-Paper.pdf>
- [20] P. Dhariwal and A. Nichol, "Diffusion models beat gans on image synthesis," in *Advances in Neural Information Processing Systems*, M. Ranzato, A. Beygelzimer, Y. Dauphin, P. Liang, and J. W. Vaughan, Eds., vol. 34. Curran Associates, Inc., 2021, pp. 8780–8794. [Online]. Available: <https://proceedings.neurips.cc/paper/2021/file/49ad23d1ec9fa4bd8d77d02681df5cfa-Paper.pdf>
- [21] H. Li, Y. Yang, M. Chang, S. Chen, H. Feng, Z. Xu, Q. Li, and Y. Chen, "Srdiff: Single image super-resolution with diffusion probabilistic models," *Neurocomputing*, vol. 479, pp. 47–59, 2022. [Online]. Available: <https://www.sciencedirect.com/science/article/pii/S0925231222000522>
- [22] A. Lugmayr, M. Danelljan, A. Romero, F. Yu, R. Timofte, and L. Van Gool, "Repaint: Inpainting using denoising diffusion probabilistic models," 2022. [Online]. Available: <https://arxiv.org/abs/2201.09865>
- [23] B. Kavar, M. Elad, S. Ermon, and J. Song, "Denoising diffusion restoration models," 2022. [Online]. Available: <https://arxiv.org/abs/2201.11793>
- [24] R. R. Coifman and D. L. Donoho, *Translation-Invariant De-Noising*, A. Antoniadis and G. Oppenheim, Eds. New York, NY: Springer New York, 1995. [Online]. Available: [https://doi.org/10.1007/978-1-4612-2544-7\\_9](https://doi.org/10.1007/978-1-4612-2544-7_9)
- [25] O. Ronneberger, P. Fischer, and T. Brox, "U-net: Convolutional networks for biomedical image segmentation," in *MICCAI*, 2015.
- [26] A. Vaswani, N. Shazeer, N. Parmar, J. Uszkoreit, L. Jones, A. N. Gomez, L. u. Kaiser, and I. Polosukhin, "Attention is all you need," in *Advances in Neural Information Processing Systems*, I. Guyon, U. V. Luxburg, S. Bengio, H. Wallach, R. Fergus, S. Vishwanathan, and R. Garnett, Eds., vol. 30. Curran Associates, Inc., 2017. [Online]. Available: <https://proceedings.neurips.cc/paper/2017/file/3f5ee243547dee91fbd053c1c4a845aa-Paper.pdf>
- [27] A. Brock, J. Donahue, and K. Simonyan, "Large scale GAN training for high fidelity natural image synthesis," in *International Conference on Learning Representations*, 2019. [Online]. Available: <https://openreview.net/forum?id=B1xsqj09Fm>
- [28] C. Zhang, P. Yue, D. Tapete, L. Jiang, B. Shangquan, L. Huang, and G. Liu, "A deeply supervised image fusion network for change detection in high resolution bi-temporal remote sensing images," *ISPRS Journal of Photogrammetry and Remote Sensing*, vol. 166, pp. 183–200, 2020. [Online]. Available: <https://www.sciencedirect.com/science/article/pii/S0924271620301532>
- [29] M. Schmitt, L. Hughes, and X. Zhu, "The sen1-2 dataset for deep learning in sar-optical data fusion," in *ISPRS Annals of Photogrammetry, Remote Sensing and Spatial Information Sciences*, vol. IV-1, 09 2018, pp. 141–146.
- [30] F. Argenti, A. Lapini, T. Bianchi, and L. Alparone, "A tutorial on speckle reduction in synthetic aperture radar images," *IEEE Geoscience and Remote Sensing Magazine*, vol. 1, no. 3, pp. 6–35, 2013.